Z. Phys. C - Particles and Fields 17, 5-15 (1983)

Zeitschrift für Physik C Particles and Fields

Charged Hadron Composition of the Final State in e^+e^- Annihilation at High Energies

TASSO Collaboration

M. Althoff, R. Brandelik[1], W. Braunschweig, K. Gather, F.J. Kirschfink, K. Lübelsmeyer, H.-U. Martyn, G. Peise, J. Rimkus, H.G. Sander, D. Schmitz, H. Siebke, D. Trines, W. Wallraff

I. Physikalisches Institut der RWTH Aachen, D-5100 Aachen, Federal Republic of Germany[11]

H. Boerner[2], H.M. Fischer, H. Hartmann, E. Hilger, W. Hillen, G. Knop, L. Köpke, H. Kolanoski, H. Kück, R. Wedemeyer, N. Wermes[3], M. Wollstadt

Physikalisches Institut der Universität Bonn, D-5300 Bonn, Federal Republic of Germany[11]

H. Burkhardt, S. Cooper, J. Franzke, H. Hultschig, P. Joos, W. Koch, U. Kötz, H. Kowalski[4], A. Ladage, B. Löhr, D. Lüke, P. Mättig, K.H. Mess, D. Notz, J. Pyrlik, D.R. Quarrie[5], R. Riethmüller, W. Schütte, P. Söding, G. Wolf, G. Yekutieli[6]

Deutsches Elektronen-Synchrotron, DESY, D-2000 Hamburg, Federal Republic of Germany

R. Fohrmann, H.L. Krasemann, P. Leu, E. Lohrmann, D. Pandoulas, G. Poelz, O. Römer[7], P. Schmüser, B.H. Wiik

II. Institut für Experimentalphysik der Universität Hamburg, D-2000 Hamburg, Federal Republic of Germany[11]

I. Al-Agil, R. Beuselinck, D.M. Binnie, A.J. Campbell, P.J. Dornan, D.A. Garbutt, T.D. Jones, W.G. Jones, S.L. Lloyd, J. McCardle, J.K. Sedgebeer

Department of Physics, Imperial College, London SW7 2AZ, England[12]

K.W. Bell[5], M.G. Bowler, I.C. Brock, R.J. Cashmore, R. Carnegie, P.E.L. Clarke, R. Devenish, P. Grossmann, J. Illingworth, G.L. Salmon, J. Thomas, T.R. Wyatt, C. Youngman

Department of Nuclear Physics, Oxford University, Oxford OX1 3RH England[12]

B. Foster, J.C. Hart, J. Harvey, J. Proudfoot, D.H. Saxon, P.L. Woodworth

Rutherford Appleton Laboratory, Chilton, Didcot, Oxon OX11 0QX, England[12]

D. Heyland, M. Holder

Gesamthochschule Siegen, D-5900 Siegen, Federal Republic of Germany

E. Duchovni, Y. Eisenberg, U. Karshon, G. Mikenberg, D. Revel, E. Ronat, A. Shapira

Weizmann Institute, Rehovot, Israel[13]

T. Barklow, J. Freeman[8], P. Lecomte[9], T. Meyer[10], G. Rudolph, H. Venkataramania, E. Wicklund, Sau Lan Wu, G. Zobernig

Department of Physics, University of Wisconsin, Madison, WI 53706, USA[14]

Received 2 November 1982

1 Now at IST, Darmstadt, Germany
2 Now at KEK, Oho-Machi, Japan
3 Now at SLAC, Stanford, CA., USA
4 On leave at CERN, Geneva, Switzerland
5 On leave from Rutherford Appleton Laboratory, Chilton, England
6 Minerva Fellow, on leave from Weizmann Institute, Rehovot, Israel
7 Now at SCS, Hamburg, Germany
8 Now at Fermilab, Batavia, Ill., USA
9 Now at ETH, Zürich, Switzerland
10 Now at Texas A+M University, Texas, USA
11 Supported by the Deutsches Bundesministerium für Forschung und Technologie
12 Supported by the UK Science and Engineering Research Council
13 Supported by the Minerva Gesellschaft für Forschung mbH
14 Supported by the US Department of Energy contract AC02-76ER00881

Abstract. The inclusive production of $\pi^{\pm}$ and $K^{\pm}$ mesons and of protons and antiprotons in e^+e^- annihilation has been measured at c.m. energies of $W=14$, 22 and 34 GeV. Using time of flight measurements and Cerenkov counters the full momentum range has been covered. Differential cross sections and total particle yields are given. At particle momenta of 0.4 GeV/c more than 90% of the charged hadrons are pions. With increasing momentum the fraction of pions among the charged hadrons decreases. At $W=34$ GeV and a momentum of 5 GeV/c the particle fractions are approximately $\pi^{\pm}:K^{\pm}:p,\bar{p}=0.55:0.3:0.15$. On average an event at $W=34$ GeV contains $10.3\pm0.4\pi^{\pm}$, $2.0\pm0.2K^{\pm}$ and $0.8\pm0.1\,p,\bar{p}$. In addition, we present results on baryon correlations using a sample of events where two or more protons and/or antiprotons are observed in the final state.

The knowledge of the particle composition of the final state in e^+e^- annihilation is important for understanding the fragmentation of quarks and gluons into hadrons. Measurements of inclusive charged pion production in the PETRA energy range [1, 2] show that the fraction of pions among the charged hadrons is high at low particle momenta but decreases to about 50% at high momenta. It is therefore expected that kaon and $p,\bar{p}$ production plays a more important rôle as the particle momentum increases. In contrast to measurements of neutral kaon and $\Lambda,\bar{\Lambda}$ inclusive spectra [3–5], data on charged kaons and $p,\bar{p}$ [2, 5] have only been available for low momenta. In the present paper we report on measurements of $\pi^{\pm}, K^{\pm}$, and $p,\bar{p}$ spectra covering essentially the whole momentum range at c.m. energies $W=14$, 22 and 34 GeV. The 34 GeV point is an average of data taken between 30 and 37 GeV.

The experiment was performed with the TASSO detector at PETRA. The present analysis is an extension of our already published study of $\pi^{\pm}$ production [1]. At $W=14$ and 22 GeV, data samples identical to those of [1] were used to determine the $K^{\pm}$ and $p,\bar{p}$ yields over a wide momentum range. At $W=34$ GeV, in addition to measuring the $K^{\pm}$ and $p,\bar{p}$ yields, we have repeated our analysis of $\pi^{\pm}$ production with a data sample that was approximately twice the size of that used in [1].

Hadronic final states from e^+e^- annihilation were selected using the information on charged particle momenta, applying the same cuts as in [6]. Charged particle momenta were measured in the central detector [7] with an accuracy of $\sigma_p/p = 0.017\cdot\sqrt{1+p^2}$ (with p in GeV/c). The contamination of our hadronic event sample is small. Beam gas scattering is found to contribute 0.5 ± 0.5% at $W=14$ GeV and is negligible at higher energies. The contribution of τ pair production is 1.5 ± 1.5% at $W=14$ GeV and 1.2 ± 1.2% at $W>14$ GeV. The background from $\gamma\gamma$ processes is at most 1.6 ± 0.8% at all energies.

The particle separation was done with the inner and the hadron arm time-of-flight counters and with Cerenkov counters. Detailed descriptions have already been published [1, 8, 9]. The inner time-of-flight system (ITOF) is located at a radial distance of 132 cm from the beam axis. It consists of 48 counters viewed by phototubes at both ends and covers a solid angle of 82% of 4π. The rms time resolution is 0.45 ns for particles passing through the center of the counters, improving approximately linearly to 0.27 ns for particles passing through near the end of the scintillators. Averaged over the whole data sample the rms time resolution was 0.38 ns. The hadron arm time-of-flight system (HATOF) is located at an average distance of 5.5 m from the interaction point and covers a solid angle of 20% of 4π. The average rms time resolution in the HATOF counters was 0.45 ns.

Figure 1a (b) shows the scatter plot of particle velocity β vs momentum in the ITOF (HATOF) counters. Clear pion, kaon and proton bands can be seen. Pions and kaons were separated in the momentum range 0.3–1.0 GeV/c in the ITOF counters and 0.5–1.5 GeV/c in the HATOF counters. Proton separation was done in the momentum range 0.4–1.4 GeV/c (1.0–2.0 GeV/c) in the ITOF (HATOF) counters.

Three types of Cerenkov counters, arranged sequentially and subtending a solid angle of 19% of 4π, were used for particle identification at higher momenta. The radiators are silica aerogel, Freon 114 and CO_2 with threshold momenta for pions of 0.7, 2.7 and 4.8 GeV/c, for kaons of 2.3, 9.5 and 17 GeV/c, and for protons of 4.4, 18 and 32 GeV/c respectively. The Cerenkov counters allowed pion identification for all momenta above 0.8 GeV/c and kaon-proton separation in the momentum range 3–6 GeV/c and for momenta above 10 GeV/c.

In order to demonstrate the performance of the Cerenkov counter system we show in Fig. 2 various Cerenkov counter rates as a function of particle momentum. Figure 2a shows the normalized aerogel counter rate $f_A=N_{\text{Aerogel}}/N_{\text{tot}}$, i.e. the number of particles in a given momentum interval which produce light in aerogel divided by the total number of particles selected for particle identification in that interval. The data shown are corrected for background

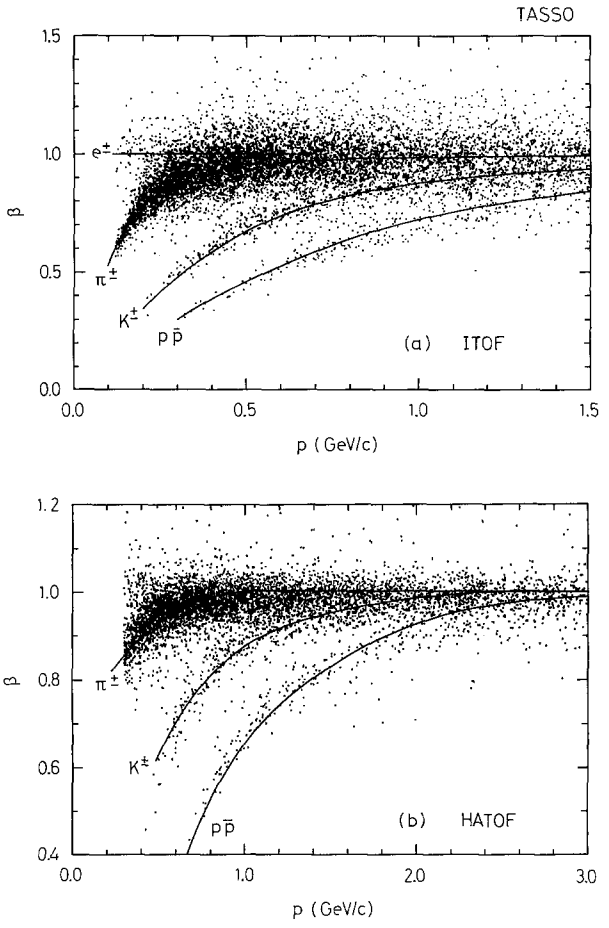

Fig. 1a and b. Particle velocity β versus momentum for tracks from multihadronic events. **a** inner time-of-flight counters, **b** hadron arm time-of-flight counters. The theoretical expectation values for different particle species are indicated by the solid lines

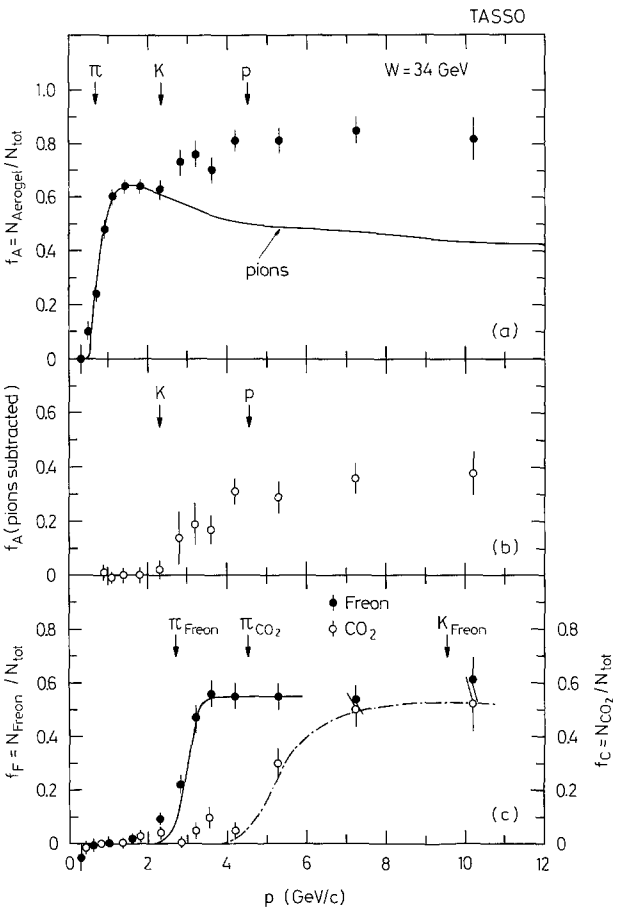

Fig. 2a–c. Fraction of tracks selected for particle identification from multihadronic events at $W=34$ GeV which produce light in the Cerenkov counters. The data are corrected for background due to electrons and non-recognized electromagnetic showers. The error bars include all statistical and systematic errors. The arrows indicate the pion, kaon and proton thresholds. **a** Aerogel counters. The solid line is the pion contribution (see text). **b** The same as in **a**, but with the pion contribution subtracted. The error bars contain also the uncertainties resulting from the error of the pion fraction. **c** Freon counters (closed circles) and CO_2 counters (open circles). The solid and dashed dotted lines are calculated pion threshold curves assuming a constant pion fraction of 0.55 in the momentum range of 2.0 to 12.0 GeV/c. Errors as in **a**

due to electrons and non-recognized showers. A steep rise is observed above 0.6 GeV/c showing the pion threshold in aerogel. This is followed by a plateau region between 1.2 and 2.3 GeV/c and then a second rise is observed above the kaon threshold. The curve in Fig. 2a shows the pion contribution to f_A which is calculated from the measured pion fractions [1] multiplied by the efficiency of the aerogel counters. The difference between f_A and this curve is shown in Fig. 2b for all momenta above 0.8 GeV/c. The rise above the kaon threshold is observed more clearly than in f_A, since the pion fraction drops with increasing momentum. With the present amount of data the proton threshold above 4.5 GeV/c is not observed.

The normalized rates of the Freon counters $f_F = N_{\text{Freon}}/N_{\text{tot}}$ and of the CO_2 counters $f_C = N_{CO_2}/N_{\text{tot}}$ are shown in Fig. 2c. The data are corrected for background due to electrons and non-recognized showers. The pion thresholds between 2.7 and 3 GeV/c in Freon and between 5 and 7 GeV/c in CO_2 are clearly seen.

The procedures employed in the TOF and Cerenkov analyses closely follow those in [1]. In this paper we describe in detail the particle separation in the momentum range 3–6 GeV/c and above 10 GeV/c.

The detection efficiencies of the Cerenkov counters for the different particle species were calculated as a function of momentum, using the efficiency plateau values as obtained from cosmic ray muons

Table 1. Mean detection efficiency of the Cerenkov counters for pions, kaons, and protons (antiprotons) in the momentum regions $3.0<p<6.0$ GeV/c and $10.0<p<17.0$ GeV/c. The uncertainty in the efficiency is ± 0.05 in the threshold regions and ± 0.02 (± 0.01) for the aerogel (Freon and CO_2) counters in the plateau region

Momentum Range (GeV/c)	Detection Efficiency					
	Aerogel			Freon		CO_2
	π	K	p	π	K	π
3.0- 3.4	0.90	0.69	–	0.77	–	–
3.4- 3.8	0.90	0.76	–	0.95	–	–
3.8- 4.6	0.90	0.81	0.09	0.99	–	0.04
4.6- 6.0	0.91	0.85	0.46	>0.99	–	0.44
10.0-17.0	0.91	0.90	0.84	>0.99	0.54	0.96

and taking into account the momentum resolution of the detector and the measured hadron momentum spectrum [10]. The efficiencies are listed in Table 1.

In the momentum range 3–6 GeV/c, pions were identified by the Freon counters whereas kaons and protons were separated on a statistical basis making use of their different detection efficiencies in the aerogel counters. More specifically, we divide the number of particles selected for the Cerenkov analysis into three classes:

- the $\bar{A}\bar{F}$ class having no light in either aerogel or Freon
- the $A\bar{F}$ class having light in aerogel but not in Freon
- the XF class having light in Freon irrespective of the aerogel response.

The number of entries in each class was corrected for background due to electrons and non-recognized showers as discussed extensively in [1]. The number of pions, kaons and protons (antiprotons) entering the Cerenkov counters N'_π, N'_K, N'_p is then related to the number of particles in the three classes $N(\bar{A}\bar{F})$, $N(A\bar{F})$, $N(XF)$ in the following way:

$$N(XF)=\eta_\pi \cdot N'_\pi,$$
$$N(\bar{A}\bar{F})=(1-\varepsilon_\pi)(1-\eta_\pi)(1-\delta_\pi)N'_\pi$$
$$+(1-\varepsilon_K)(1-\delta_K)N'_K+(1-\varepsilon_p)(1-\delta_p)N'_p,$$
$$N(A\bar{F})=[\varepsilon_\pi+(1-\varepsilon_\pi)\delta_\pi](1-\eta_\pi)N'_\pi$$
$$+[\varepsilon_K+(1-\varepsilon_K)\delta_K]N'_K+[\varepsilon_p+(1-\varepsilon_p)\delta_p]N'_p.$$

Here η_π is the pion efficiency to produce light in the Freon counters, ε_π, ε_K, ε_p is the pion, kaon, proton efficiency to produce light in aerogel, and δ_π, δ_K, δ_p is the probability that a pion, kaon, proton will produce light in aerogel through knock-on electrons*.

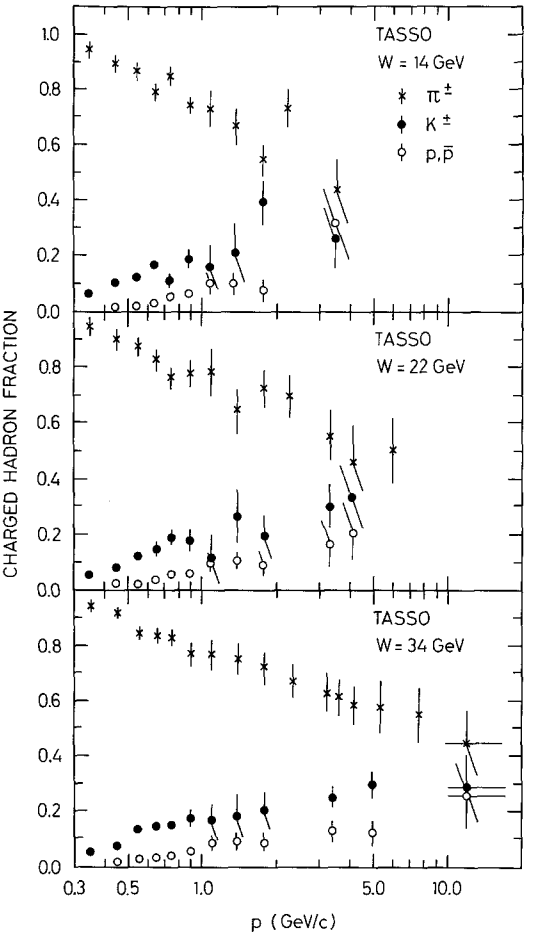

Fig. 3. Fraction of $\pi^\pm$, $K^\pm$, $p,\bar{p}$ as a function of particle momentum at c.m. energies $W=14$, 22 and 34 GeV

For momenta above 10 GeV/c a similar analysis was carried out using the CO_2 counters to identify pions (detection efficiency 0.96) and the Freon counters to separate kaons (average detection efficiency 0.54) from protons (antiprotons). The low value of the kaon efficiency in Freon reflects the apparent broadening of the Cerenkov threshold region resulting from the finite momentum resolution.

To derive the particle fractions $f_i=N_i/N_{h^\pm}$, where $i=\pi^\pm$, $K^\pm$, $p,\bar{p}$ and $N_{h^\pm}$ is the number of charged hadrons in each momentum interval, the numbers N'_π, N'_K and N'_p were corrected for the decay of pions and kaons, for nuclear interactions in the

* The probabilities δ_π, δ_K and δ_p contain roughly equal contributions from the magnet coil and the aerogel material. In the momentum region between 3.0 and 6.0 GeV/c, $\delta_\pi \sim 6.5\%$, δ_K ranges from 5 to 6.5%, while δ_p varies from 1 to 5.5%. The contribution of knock-on electrons to the Freon rate and thus to the number of pions is negligible

material in front of the counters, and for the contamination due to muons. Within statistical errors equal numbers of positive and negative particles were observed for each particle species at all momenta and c.m. energies. We also verified that the tracks selected for particle identification have the same spectra in momentum and transverse momentum with respect to the sphericity axis as all central detector tracks. Furthermore, the events in which tracks were selected for particle identification have the same sphericity and multiplicity distributions as the total hadronic event sample. The results of the ITOF, HATOF, and Cerenkov analyses are in good agreement in the regions of overlap and were combined.

The particle fractions are shown in Fig. 3 as a function of particle momentum for the three c.m. energies $W=14$, 22 and 34 GeV and listed in Tables 2–4. The particle fractions include the contributions from decay products of particles with a lifetime smaller than $3\cdot10^{-10}$ s. For example, the pion fractions include the contribution from $K_s^0\to\pi^+\pi^-$ decays and the proton fractions include contributions from Λ decays. The particle fractions are in good agreement with our previous lower statistics results [1, 2]. The kaon fraction in the 1.4–2.0 GeV/c interval (1.0–2.0 GeV/c for $W=22$ GeV) was not directly measured, but was inferred from the values of f_π and f_p.

For all three c.m. energies, at low particle momenta most of the charged hadrons produced are pions (more than 90% at 0.4 GeV/c). At higher momenta, kaon and $p,\bar{p}$ production become increasingly important: the pion fraction decreases smooth-

Table 2. Charged hadron inclusive cross sections for $W=14$ GeV

a) $\pi^+ + \pi^-$

p (GeV/c)	<p> (GeV/c)	fraction	dσ/dp (nbarn/GeV/c)	x	<x>	s/β·dσ/dx (μbarn·GeV²)	<E> (GeV)	E/4πp²·dσ/dp (nbarn·GeV⁻²c³)
0.3 - 0.4	0.35	0.94 ± 0.03	16.6 ± 0.97	0.047 - 0.061	0.054	26.4 ± 1.55	0.38	4.07 ± 0.24
0.4 - 0.5	0.45	0.89 ± 0.03	14.6 ± 0.74	0.061 - 0.074	0.067	21.9 ± 1.11	0.47	2.70 ± 0.14
0.5 - 0.6	0.55	0.86 ± 0.03	11.5 ± 0.56	0.074 - 0.088	0.081	16.8 ± 0.83	0.57	1.72 ± 0.08
0.6 - 0.7	0.65	0.79 ± 0.03	8.71 ± 0.46	0.088 - 0.102	0.095	12.5 ± 0.66	0.66	1.09 ± 0.058
0.7 - 0.8	0.75	0.85 ± 0.04	8.06 ± 0.49	0.102 - 0.116	0.109	11.5 ± 0.70	0.76	0.87 ± 0.053
0.8 - 1.0	0.90	0.74 ± 0.03	5.48 ± 0.30	0.116 - 0.144	0.130	7.69 ± 0.41	0.91	0.490 ± 0.027
1.0 - 1.2	1.1	0.73 ± 0.07	3.95 ± 0.40	0.144 - 0.17	0.158	5.50 ± 0.56	1.11	0.288 ± 0.029
1.2 - 1.6	1.4	0.66 ± 0.07	2.34 ± 0.27	0.17 - 0.23	0.20	3.24 ± 0.37	1.4	0.135 ± 0.016
1.6 - 2.0	1.8	0.54 ± 0.06	1.16 ± 0.14	0.23 - 0.29	0.26	1.60 ± 0.20	1.8	0.052 ± 0.006
2.0 - 2.6	2.3	0.73 ± 0.07	0.90 ± 0.11	0.29 - 0.37	0.33	1.25 ± 0.15	2.3	0.032 ± 0.004
3.0 - 4.6	3.6	0.43 ± 0.12	0.10 ± 0.03	0.43 - 0.66	0.51	0.14 ± 0.04	3.6	0.0023± 0.0007

b) $K^+ + K^-$

p (GeV/c)	<p> (GeV/c)	fraction	dσ/dp (nbarn/GeV/c)	x	<x>	s/β·dσ/dx μbarn·GeV²	<E> (GeV)	E/4πp²·dσ/dp (nbarn·GeV⁻²c³)
0.3 - 0.4	0.35	0.059± 0.010	1.04 ± 0.18	0.083 - 0.091	0.087	4.29 ± 0.76	0.61	0.410 ± 0.073
0.4 - 0.5	0.45	0.098± 0.011	1.61 ± 0.19	0.091 - 0.101	0.096	4.87 ± 0.58	0.67	0.422 ± 0.050
0.5 - 0.6	0.55	0.12 ± 0.02	1.61 ± 0.18	0.101 - 0.111	0.106	4.00 ± 0.45	0.74	0.314 ± 0.035
0.6 - 0.7	0.65	0.17 ± 0.02	1.87 ± 0.27	0.111 - 0.122	0.117	4.06 ± 0.59	0.82	0.288 ± 0.042
0.7 - 0.8	0.75	0.11 ± 0.02	1.05 ± 0.20	0.122 - 0.134	0.128	2.07 ± 0.40	0.90	0.133 ± 0.026
0.8 - 1.0	0.90	0.19 ± 0.04	1.42 ± 0.30	0.134 - 0.16	0.147	2.53 ± 0.54	1.03	0.143 ± 0.031
1.0 - 1.6	1.3	0.18 ± 0.07	0.80 ± 0.29	0.16 - 0.24	0.20	1.27 ± 0.47	1.39	0.053 ± 0.021
1.6 - 2.0	1.8	0.39 ± 0.08	0.84 ± 0.18	0.24 - 0.29	0.27	1.24 ± 0.26	1.85	0.039 ± 0.008
3.0 - 4.6	3.6	0.26 ± 0.11	0.06 ± 0.03	0.43 - 0.66	0.52	0.09 ± 0.04	3.6	0.0014± 0.0006

c) $p+\bar{p}$

p (GeV/c)	<p> (GeV/c)	fraction	dσ/dp (nbarn/GeV/c)	x	<x>	s/β·dσ/dx (μbarn·GeV²)	<E> (GeV)	E/4πp²·dσ/dp (nbarn·GeV⁻²c³)
0.4 - 0.5	0.45	0.013± 0.004	0.21 ± 0.07	0.145 - 0.151	0.148	1.55 ± 0.48	1.04	0.087 ± 0.027
0.5 - 0.6	0.55	0.016± 0.005	0.21 ± 0.07	0.151 - 0.159	0.155	1.14 ± 0.36	1.08	0.061 ± 0.019
0.6 - 0.7	0.65	0.032± 0.008	0.35 ± 0.09	0.159 - 0.167	0.163	1.49 ± 0.38	1.14	0.076 ± 0.019
0.7 - 0.8	0.75	0.052± 0.012	0.50 ± 0.12	0.167 - 0.176	0.171	1.74 ± 0.41	1.20	0.084 ± 0.020
0.8 - 1.0	0.90	0.063± 0.013	0.47 ± 0.10	0.176 - 0.196	0.185	1.34 ± 0.28	1.30	0.060 ± 0.013
1.0 - 1.2	1.10	0.10 ± 0.03	0.54 ± 0.16	0.196 - 0.22	0.206	1.28 ± 0.39	1.44	0.051 ± 0.016
1.2 - 1.6	1.4	0.10 ± 0.03	0.35 ± 0.12	0.22 - 0.27	0.24	0.71 ± 0.24	1.67	0.025 ± 0.008
1.6 - 2.0	1.8	0.07 ± 0.04	0.16 ± 0.09	0.27 - 0.32	0.29	0.27 ± 0.15	2.0	0.008 ± 0.004
3.0 - 4.6	3.6	0.31 ± 0.13	0.073± 0.033	0.45 - 0.67	0.53	0.11 ± 0.05	3.7	0.0017± 0.0008

Table 3. Charged hadron inclusive cross sections for $W=22$ GeV

a) $n^+ + \pi^-$

p (GeV/c)	<p> (GeV/c)	fraction	$d\sigma/dp$ (nbarn/GeV/c)	x	<x>	$s/\beta \cdot d\sigma/dx$ (μbarn·GeV^2)	<E> (GeV)	$E/4\pi p^2 \cdot d\sigma/dp$ (nbarn·GeV$^{-2}c^3$)
0.3 - 0.4	0.35	0.95 ± 0.04	6.85 ± 0.44	0.030 - 0.039	0.034	42.3 ± 2.7	0.38	1.68 ± 0.11
0.4 - 0.5	0.45	0.90 ± 0.04	5.83 ± 0.35	0.039 - 0.047	0.043	34.1 ± 2.1	0.47	1.08 ± 0.07
0.5 - 0.6	0.55	0.87 ± 0.04	4.74 ± 0.28	0.047 - 0.056	0.052	26.8 ± 1.6	0.57	0.71 ± 0.04
0.6 - 0.7	0.65	0.83 ± 0.04	4.15 ± 0.26	0.056 - 0.065	0.060	23.1 ± 1.5	0.66	0.52 ± 0.03
0.7 - 0.8	0.75	0.76 ± 0.04	3.26 ± 0.22	0.065 - 0.074	0.069	18.0 ± 1.2	0.76	0.35 ± 0.02
0.8 - 1.0	0.90	0.77 ± 0.05	2.62 ± 0.19	0.074 - 0.092	0.083	14.3 ± 1.0	0.91	0.24 ± 0.02
1.0 - 1.2	1.10	0.78 ± 0.09	2.01 ± 0.25	0.092 - 0.110	0.101	10.9 ± 1.3	1.11	0.15 ± 0.02
1.2 - 1.6	1.4	0.64 ± 0.08	1.10 ± 0.15	0.110 - 0.146	0.127	5.9 ± 0.8	1.4	0.063 ± 0.008
1.6 - 2.0	1.8	0.72 ± 0.07	0.83 ± 0.09	0.146 - 0.18	0.163	4.43 ± 0.50	1.8	0.037 ± 0.004
2.0 - 2.6	2.3	0.39 ± 0.08	0.53 ± 0.07	0.18 - 0.24	0.21	2.84 ± 0.38	2.3	0.019 ± 0.003
3.0 - 3.8	3.4	0.55 ± 0.10	0.18 ± 0.04	0.27 - 0.35	0.30	0.94 ± 0.19	3.4	0.0042± 0.0008
3.8 - 4.6	4.1	0.47 ± 0.12	0.065± 0.018	0.35 - 0.42	0.38	0.35 ± 0.10	4.1	0.0012± 0.0003
4.6 - 10.0	6.0	0.50 ± 0.12	0.020± 0.006	0.42 - 0.91	0.55	0.11 ± 0.03	6.0	0.0003± 0.0001

b) $K^+ + K^-$

p (GeV/c)	<p> (GeV/c)	fraction	$d\sigma/dp$ (nbarn/GeV/c)	x	<x>	$s/\beta \cdot d\sigma/dx$ (μbarn·GeV^2)	<E> (GeV)	$E/4\pi p^2 \cdot d\sigma/dp$ (nbarn·GeV$^{-2}c^3$)
0.3 - 0.4	0.35	0.053± 0.011	0.38 ± 0.08	0.053 - 0.058	0.055	6.12 ± 1.31	0.61	0.151 ± 0.032
0.4 - 0.5	0.45	0.081± 0.014	0.54 ± 0.09	0.058 - 0.064	0.061	6.18 ± 1.10	0.67	0.138 ± 0.025
0.5 - 0.6	0.55	0.12 ± 0.02	0.64 ± 0.10	0.064 - 0.071	0.067	6.15 ± 0.92	0.74	0.124 ± 0.019
0.6 - 0.7	0.65	0.14 ± 0.02	0.72 ± 0.10	0.071 - 0.078	0.074	6.04 ± 0.86	0.82	0.111 ± 0.016
0.7 - 0.8	0.75	0.19 ± 0.03	0.82 ± 0.11	0.078 - 0.086	0.082	6.21 ± 0.86	0.90	0.103 ± 0.014
0.8 - 1.0	0.90	0.17 ± 0.04	0.59 ± 0.12	0.086 - 0.10	0.093	4.09 ± 0.83	1.03	0.060 ± 0.012
1.0 - 1.6	1.3	0.18 ± 0.07	0.39 ± 0.15	0.10 - 0.15	0.125	2.41 ± 0.94	1.40	0.026 ± 0.011
1.6 - 2.0	1.8	0.19 ± 0.08	0.22 ± 0.09	0.15 - 0.19	0.17	1.25 ± 0.53	1.85	0.010 ± 0.004
3.0 - 3.8	3.4	0.29 ± 0.09	0.092± 0.030	0.28 - 0.35	0.31	0.50 ± 0.16	3.4	0.0022± 0.0007
3.8 - 4.6	4.1	0.33 ± 0.12	0.045± 0.017	0.35 - 0.42	0.38	0.25 ± 0.09	4.2	0.0009± 0.0003

c) $p + \bar{p}$

p (GeV/c)	<p> (GeV/c)	fraction	$d\sigma/dp$ (nbarn/GeV/c)	x	<x>	$s/\beta \cdot d\sigma/dx$ (μbarn·GeV^2)	<E> (GeV)	$E/4\pi p^2 \cdot d\sigma/dp$ (nbarn·GeV$^{-2}c^3$)
0.4 - 0.5	0.45	0.020± 0.007	0.13 ± 0.05	0.092 - 0.096	0.094	3.7 ± 1.3	1.04	0.053 ± 0.019
0.5 - 0.6	0.55	0.015± 0.007	0.08 ± 0.04	0.096 - 0.101	0.099	1.7 ± 0.8	1.08	0.023 ± 0.011
0.6 - 0.7	0.65	0.032± 0.010	0.16 ± 0.05	0.101 - 0.106	0.104	2.6 ± 0.8	1.14	0.035 ± 0.011
0.7 - 0.8	0.75	0.052± 0.013	0.22 ± 0.06	0.106 - 0.112	0.109	3.0 ± 0.8	1.20	0.038 ± 0.010
0.8 - 1.2	1.00	0.065± 0.013	0.21 ± 0.04	0.112 - 0.138	0.125	2.1 ± 0.4	1.37	0.023 ± 0.004
1.2 - 1.6	1.4	0.10 ± 0.03	0.18 ± 0.04	0.138 - 0.17	0.152	1.4 ± 0.3	1.67	0.012 ± 0.003
1.6 - 2.0	1.8	0.09 ± 0.04	0.10 ± 0.05	0.17 - 0.20	0.18	0.70 ± 0.31	2.0	0.0052± 0.0023
3.0 - 3.8	3.4	0.16 ± 0.09	0.051± 0.028	0.29 - 0.36	0.32	0.29 ± 0.16	3.5	0.0013± 0.0007
3.8 - 4.6	4.1	0.20 ± 0.11	0.028± 0.015	0.36 - 0.43	0.39	0.15 ± 0.09	4.2	0.0005± 0.0003

ly to about 50%, while f_K and f_p increase to about 30% and 20%, respectively.

The cross section $d\sigma/dp$ for the inclusive production of charged hadrons, $e^+e^- \to h^\pm X$, has been measured by using the central detector data [10]. We computed the cross sections $(d\sigma/dp)_i$ for production of the different particle species by multiplying these values with the particle fractions f_i.

The scaled cross sections $s/\beta\, d\sigma/dx$ ($s=W^2$, $\beta = p_i/E_i$, $x=2E_i/W$) are shown for $W=14$, 22 and 34 GeV in Figs. 4a, b, c for $\pi^\pm$, $K^\pm$ and $p, \bar{p}$ respectively. All statistical and systematic errors are included in the error bars except for an overall normalization of 8.5% at $W=14$ GeV, 6.3% at $W=22$ GeV and 5.5% at $W=34$ GeV. For $x \gtrsim 0.1$ the cross sections do not show a significant energy variation between 14 and 34 GeV. In the case of pions and kaons in this x range, they are systematically lower than the 5.2 GeV data from DASP [11], which are also shown in Fig. 4 (see also [1]).

In Fig. 5 we compare the 34 GeV $\pi^\pm$, $K^\pm$, and $p, \bar{p}$ data. The scaled cross sections for all particle types have a similar x dependence for values of $x > 0.1$. A summary of our results is given in Tables 2, 3 and 4.

The average number of charged hadrons per

Table 4. Charged hadron inclusive cross sections for $W=34$ GeV

a) $n^+ + \pi^-$

p (GeV)	<p> (GeV/c)	fraction	dσ/dp (nbarn/GeV/c)	x	<x>	s/β·dσ/dx (μbarn·GeV²)	<E> (GeV)	E/4πp²·dσ/dp (nbarn·GeV⁻²c³)
0.3 - 0.4	0.35	0.94 ± 0.02	2.97 ± 0.15	0.019 - 0.025	0.022	67.8 ± 3.4	0.38	0.728 ± 0.036
0.4 - 0.5	0.45	0.92 ± 0.02	2.65 ± 0.11	0.025 - 0.031	0.028	57.2 ± 2.4	0.47	0.491 ± 0.020
0.5 - 0.6	0.55	0.84 ± 0.02	2.27 ± 0.09	0.031 - 0.036	0.033	47.5 ± 1.8	0.57	0.339 ± 0.013
0.6 - 0.7	0.65	0.83 ± 0.02	1.90 ± 0.08	0.036 - 0.042	0.039	39.1 ± 1.5	0.66	0.238 ± 0.009
0.7 - 0.8	0.75	0.83 ± 0.03	1.66 ± 0.07	0.042 - 0.048	0.045	33.7 ± 1.5	0.76	0.179 ± 0.008
0.8 - 1.0	0.90	0.76 ± 0.04	1.27 ± 0.07	0.048 - 0.059	0.054	25.5 ± 1.5	0.91	0.114 ± 0.007
1.0 - 1.2	1.10	0.77 ± 0.06	0.97 ± 0.08	0.059 - 0.071	0.065	19.4 ± 1.6	1.11	0.071 ± 0.006
1.2 - 1.6	1.4	0.75 ± 0.06	0.68 ± 0.06	0.071 - 0.094	0.082	13.5 ± 1.2	1.41	0.039 ± 0.003
1.6 - 2.0	1.8	0.71 ± 0.06	0.47 ± 0.04	0.094 - 0.118	0.106	9.30 ± 0.86	1.8	0.021 ± 0.002
2.0 - 2.6	2.3	0.68 ± 0.06	0.31 ± 0.03	0.118 - 0.153	0.135	6.15 ± 0.58	2.3	0.011 ± 0.001
3.0 - 3.4	3.2	0.63 ± 0.07	0.15 ± 0.02	0.18 - 0.20	0.19	3.03 ± 0.36	3.2	0.0038 ± 0.0005
3.4 - 3.8	3.6	0.61 ± 0.06	0.118 ± 0.013	0.20 - 0.22	0.21	2.33 ± 0.25	3.6	0.0026 ± 0.0003
3.8 - 4.6	4.1	0.58 ± 0.07	0.066 ± 0.009	0.22 - 0.27	0.24	1.29 ± 0.17	4.1	0.0013 ± 0.0002
4.6 - 6.0	5.3	0.57 ± 0.10	0.052 ± 0.010	0.27 - 0.35	0.31	1.03 ± 0.20	5.3	0.0008 ± 0.0001
6.0 -10.0	7.6	0.55 ± 0.10	0.015 ± 0.003	0.35 - 0.59	0.45	0.29 ± 0.06	7.6	0.00016± 0.00004
10.0 -17.0	11.7	0.45 ± 0.12	0.0042± 0.0012	0.59 - 1.00	0.69	0.083 ± 0.024	11.7	0.00003± 0.00001

b) $K^+ + K^-$

p (GeV/c)	<p> (GeV/c)	fraction	dσ/dp (nbarn/GeV/c)	x	<x>	s/β·dσ/dx (μbarn·GeV²)	<E> (GeV)	E/4πp²·dσ/dp (nbarn·GeV⁻²c³)
0.3 - 0.4	0.35	0.050± 0.006	0.16 ±0.02	0.034 -0.037	0.036	9.28 ± 1.19	0.61	0.062 ± 0.008
0.4 - 0.5	0.45	0.075± 0.007	0.22 ±0.02	0.037 -0.041	0.039	9.44 ± 0.95	0.67	0.057 ± 0.006
0.5 - 0.6	0.55	0.13 ± 0.010	0.36 ±0.03	0.041 -0.046	0.044	12.7 ± 1.0	0.74	0.070 ± 0.006
0.6 - 0.7	0.65	0.14 ± 0.02	0.32 ±0.04	0.046 -0.050	0.048	9.8 ± 1.1	0.82	0.049 ± 0.006
0.7 - 0.8	0.75	0.14 ± 0.02	0.28 ±0.04	0.050 -0.055	0.053	7.9 ± 1.2	0.90	0.036 ± 0.005
0.8 - 1.0	0.90	0.17 ± 0.03	0.28 ±0.05	0.055 -0.066	0.060	7.2 ± 1.3	1.05	0.029 ± 0.005
1.0 - 1.6	1.3	0.17 ± 0.05	0.18 ±0.06	0.066 -0.099	0.082	4.0 ± 1.3	1.4	0.012 ± 0.004
1.6 - 2.0	1.8	0.20 ± 0.07	0.13 ±0.05	0.099 -0.121	0.109	2.8 ± 1.0	1.9	0.0061 ± 0.0022
3.0 - 3.8	3.4	0.24 ± 0.04	0.049 ±0.010	0.18 -0.23	0.20	0.98 ± 0.20	3.4	0.0011 ± 0.0002
3.8 - 6.0	4.7	0.28 ± 0.05	0.028 ±0.005	0.23 -0.35	0.28	0.60 ± 0.11	4.7	0.0005 ± 0.0001
10.0 -17.0	11.7	0.29 ± 0.12	0.0027±0.0011	0.59 -1.00	0.69	0.053± 0.022	11.7	0.00002± 0.00001

c) $p + \bar{p}$

p (GeV/c)	<p> (GeV/c)	fraction	dσ/dp (nbarn/GeV/c)	x	<x>	s/β·dσ/dx (μbarn·GeV²)	<E> (GeV)	E/4πp²·dσ/dp (nbarn·GeV⁻²c³)
0.4 - 0.5	0.45	0.010± 0.002	0.029 ± 0.006	0.060 - 0.062	0.061	3.03 ± 0.62	1.04	0.012 ± 0.002
0.5 - 0.6	0.55	0.023± 0.004	0.062 ± 0.011	0.062 - 0.065	0.064	4.73 ± 0.84	1.08	0.018 ± 0.003
0.6 - 0.7	0.65	0.029± 0.005	0.066 ± 0.012	0.065 - 0.069	0.067	4.00 ± 0.70	1.14	0.014 ± 0.003
0.7 - 0.8	0.75	0.033± 0.007	0.066 ± 0.014	0.069 - 0.072	0.071	3.32 ± 0.71	1.20	0.011 ± 0.002
0.8 - 1.2	1.00	0.057± 0.011	0.089 ± 0.016	0.072 - 0.089	0.081	3.41 ± 0.57	1.37	0.010 ± 0.002
1.2 - 1.6	1.4	0.090± 0.030	0.082 ± 0.027	0.089 - 0.109	0.098	2.33 ± 0.78	1.67	0.0056 ± 0.0019
1.6 - 2.0	1.8	0.085± 0.030	0.056 ± 0.020	0.109 - 0.128	0.119	1.41 ± 0.50	2.0	0.0028 ± 0.0010
3.0 - 3.8	3.4	0.12 ± 0.04	0.028 ± 0.009	0.19 - 0.23	0.21	0.59 ± 0.18	3.5	0.0007 ± 0.0002
3.8 - 6.0	4.7	0.12 ± 0.05	0.013 ± 0.005	0.23 - 0.36	0.28	0.26 ± 0.10	4.8	0.0002 ± 0.0001
10.0 -17.0	11.7	0.26 ± 0.12	0.0024± 0.0011	0.59 - 1.00	0.69	0.047± 0.022	11.7	0.000016± 0.00001

event $\langle n_i^{\pm} \rangle$ was calculated according to

$$\langle n_i^{\pm} \rangle = \frac{\int_0^{p_{\max}} \left(\frac{d\sigma}{dp}\right)_i dp}{\sigma_{\text{tot}}}$$

where σ_{tot} is the total hadronic cross section as measured in this experiment [6].

The extrapolation of $(d\sigma/dp)_i$ to zero momentum, as well as the interpolation over the momentum intervals for which particles were not identified, was done by parametrising the invariant cross sections in the form

$$(E_i/4\pi p_i^2)(d\sigma/dp)_i = \sum_m A_{im} \exp(-B_{im} E_i).$$

Two exponential terms are necessary to describe the $\pi^{\pm}$ distributions at $W=14$ and 22 GeV as well as the $K^{\pm}$ and $p, \bar{p}$ results at $W=34$ GeV. For the $\pi^{\pm}$ measurements at $W=34$ GeV the addition of a

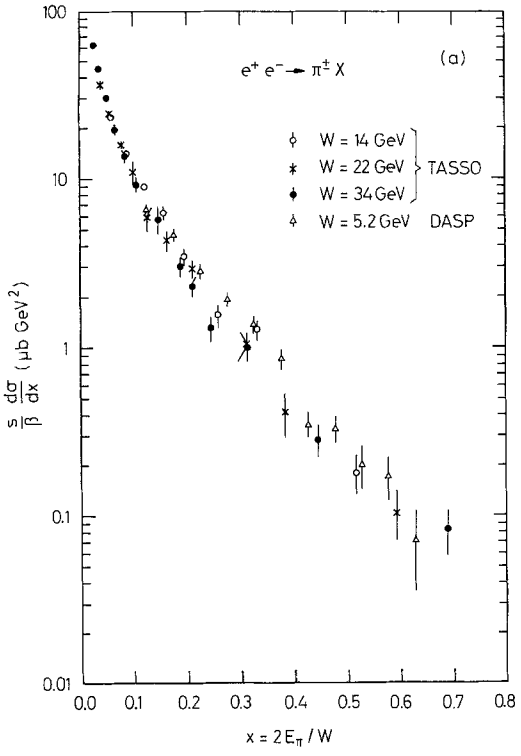

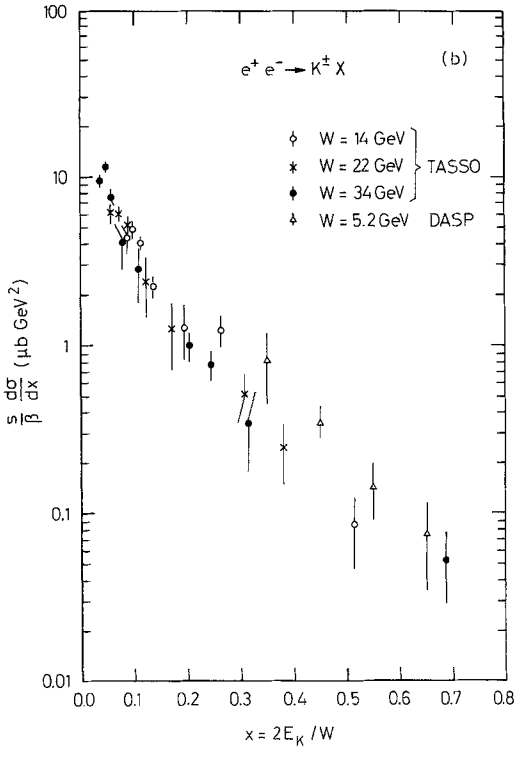

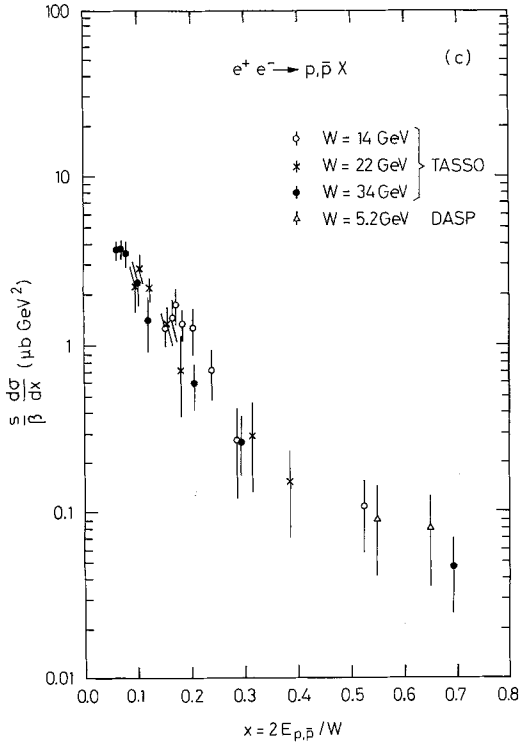

Fig. 4a–c. Scaled cross sections $(s/\beta)d\sigma/dx$ as a function of x for c.m. energies $W=14$, 22 and 34 GeV. Also shown are the DASP data [11] at $W=5.2$ GeV. **a** $\pi^{\pm}$, **b** $K^{\pm}$, **c** $p,\bar{p}$

third exponential is required to obtain a satisfactory description of the data for momenta above 5 GeV/c. In all other cases the data are well represented within their errors by a single exponential. The invariant cross sections for $\pi^{\pm}$, $K^{\pm}$, and $p,\bar{p}$ at $W=34$ GeV are shown in Fig. 6 together with the results of the fits. The values of all fitted parameters are summarized in Table 5. The fraction of the cross section determined by extrapolation is 25% in the worst case ($\pi^{\pm}$ data at $W=14$ GeV). At $W=34$ GeV it amounts to 17% for the $\pi^{\pm}$ data, 3% for $K^{\pm}$, and 2% for $p,\bar{p}$.

Figure 7 shows the average number of particles $\langle n_i^{\pm}\rangle$ produced per event as a function of the c.m. energy W. As before, the numbers contain contributions from decay products of particles with lifetimes smaller than $3\cdot 10^{-10}$ s. Also included in Fig. 7 are results from other experiments at lower energies [11–13]*. We find that on average an event at $W=34$ GeV contains $10.3\pm0.4\pi^{\pm}$, $2.0\pm0.2K^{\pm}$ and $0.8\pm0.1p,\bar{p}$. The corresponding numbers at $W=14$ GeV are 7.2 ± 0.6, 1.2 ± 0.14 and 0.42 ± 0.06, respectively. From our previous measurement [3] of

* Note that the low energy data on $\langle n_{p,\bar{p}}\rangle$ from MARK II [13], shown in Fig. 7, are somewhat higher than the values obtained previously by the MARK I experiment [14]

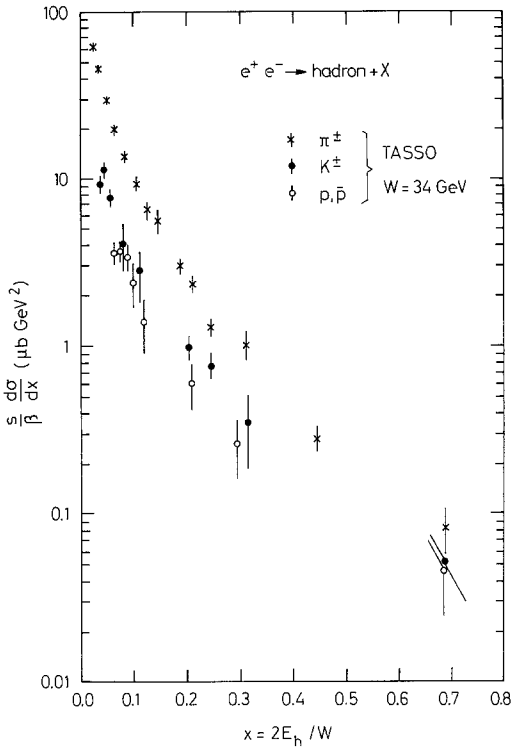

Fig. 5. Scaled cross section $(s/\beta)\,d\sigma/dx$ as a function of x at $W=34$ GeV for $\pi^{\pm}$, $K^{\pm}$ and $p,\bar{p}$

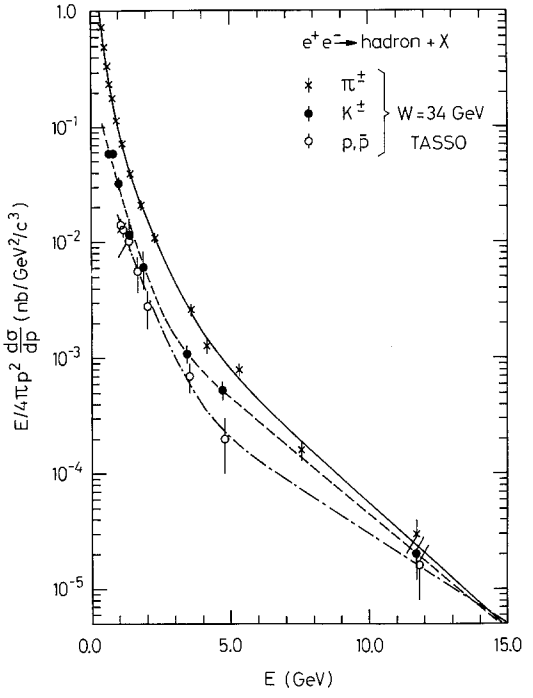

Fig. 6. Invariant cross section $(E/4\pi p^2)\,d\sigma/dp$ as a function of particle energy at $W=34$ GeV for $\pi^{\pm}$, $K^{\pm}$ and $p,\bar{p}$. The curves represent the results of the fit described in the text for pions (solid line), kaons (dashed line), protons and antiprotons (dashed-dotted line)

$\langle n_{\Lambda,\bar{\Lambda}}\rangle = 0.28 \pm 0.04$ (statistical error) ± 0.04 (systematic error) at $W=33$ GeV we conclude that about 25% of the protons originate from Λ-decays at $W=34$ GeV.

In order to obtain additional information on baryon production, we investigated events in which two or more protons and/or antiprotons were detected. For this analysis the $p,\bar{p}$ were restricted to the range 0.4–1.2 GeV/c. A proton was defined as a track with mass-squared between 0.6 and 1.4 GeV^2. For momenta below 1.0 GeV/c, the background from other particles is less than 3%, while between 1.0 and 1.2 GeV/c the background is ~5%. The observed numbers of events with two or more $p,\bar{p}$ are given in Table 6.

At $W=34$ GeV, 47 events with one proton and one antiproton ("$p+\bar{p}$" class) are observed but only 18 events with either two protons or two antipro-

Table 5. Fits to the invariant cross sections $(E/4\pi p^2)\,d\sigma/dp = \sum_m A_m \exp(-B_m E)$ for $\pi^{\pm}$, $K^{\pm}$ and $p,\bar{p}$ production; A_m in (nbarn · GeV$^{-2}\cdot c^3$), B_m in (GeV^{-1}), $m=1,2,3$

	W (GeV)	A_1	B_1	A_2	B_2	A_3	B_3	χ^2/d.o.f.
$\pi^{\pm}$	14	23.9 ±3.9	5.25±0.43	1.44 ±0.42	1.78±0.14	–	–	9.3/7
	22	8.0 ±1.2	4.70±0.32	0.36 ±0.08	1.30±0.10	–	–	7.1/9
	34	3.7 ±0.6	4.97±0.45	0.27 ±0.09	1.51±0.21	0.008±0.005	0.50±0.08	5.5/9
$K^{\pm}$	14	1.31±0.2	2.05±0.16	–	–	–	–	17.6/6
	22	0.40±0.05	1.67±0.12	–	–	–	–	12.7/9
	34	0.25±0.05	2.13±0.27	0.005±0.002	0.46±0.06	–	–	8.2/4
$p,\bar{p}$	14	0.61±0.24	1.87±0.28	–	–	–	–	6.7/7
	22	0.17±0.06	1.51±0.21	–	–	–	–	6.4/10
	34	0.07±0.03	1.58±0.35	0.001±0.001	0.36±0.11	–	–	1.6/4

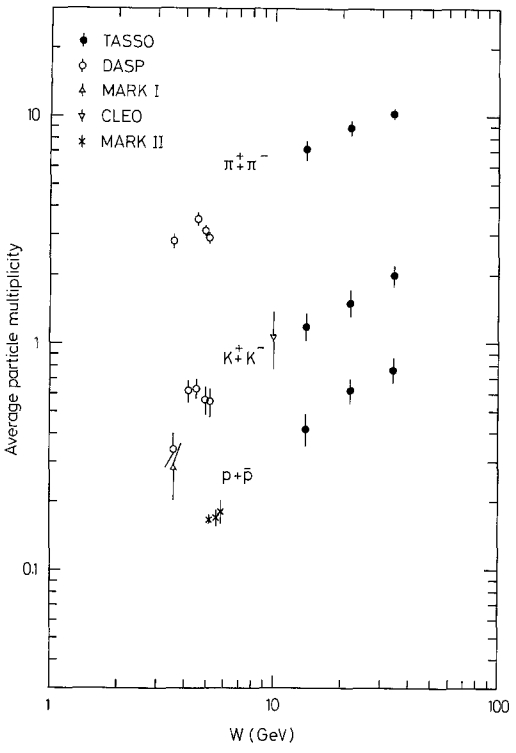

Fig. 7. Average particle multiplicity for $\pi^{\pm}$, $K^{\pm}$ and $p,\bar{p}$ as a function of c.m. energy W. The data at $W=14$, 22 and 34 GeV are from this experiment. The data at lower c.m. energies are from [11-13]

Table 6. Number of events with two or more protons and/or antiprotons detected

W (GeV/c)	Total number of hadronic events	$(p+\bar{p})$ events	$(2p)$ or $(2\bar{p})$ events	$(2p+1\bar{p})$ or $(1p+2\bar{p})$ events
14	2,704	19	3	0
22	2,120	6	1	1
34	19,676	47	18	2

tons ("$2p$" or "$2\bar{p}$" class). The background due to incorrect particle identification is about 4 events for both classes, as estimated by Monte Carlo calculations which use the same model [15, 16] as in our previous analyses [6] and which follow the generated particles through the detector.

Using events which contain at least one proton and one antiproton we studied the angular distributions of the baryons with respect to each other, both for the space angle $\theta_{p\bar{p}}$ between the proton and antiproton directions and for the azimuthal angle $\Delta\phi$ in the plane perpendicular to the thrust axis.

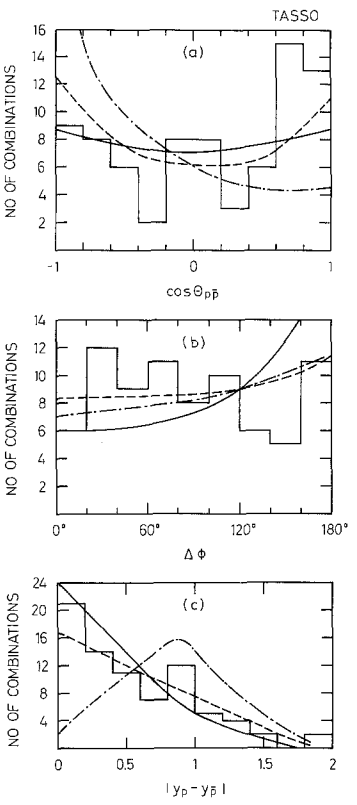

Fig. 8a–c. Proton-antiproton correlations for events with at least one observed proton and antiproton. The data from all three c.m. energies have been combined. For events with $2p+1\bar{p}$ or $1p+2\bar{p}$ both $p\bar{p}$-combinations are plotted. **a** $\cos\theta_{p\bar{p}}$, where $\theta_{p\bar{p}}$ is the angle between p and $\bar{p}$, **b** difference of azimuthal angle $\Delta\phi$ of p and $\bar{p}$, measured in the plane perpendicular to the jet axis, **c** difference of p and $\bar{p}$ in rapidity. The curves are the prediction of the models of [16] (solid line), [17] (dashed line) and [18, 19] (dashed-dotted line)

Figure 8a shows the distribution of $\cos\theta_{p\bar{p}}$. The data from all c.m. energies have been added together. The data show some enhancement at $\cos\theta_{p\bar{p}}=+1$ but are also consistent with a flat distribution. From the number of combinations with $\cos\theta_{p\bar{p}}<0$ it would appear unlikely that the proton and antiproton are always confined to the same jet. It must be noted, however, that in our limited momentum range there is a large uncertainty in associating a particle with a particular jet. Figure 8b shows the difference in azimuthal angle in the plane perpendicular to the thrust axis. Here we obtain a rather flat distribution which in particular does not show a pronounced peak at $\Delta\phi=180°$; so, in contrast to the claim made in [5], we do not observe a large angular anti-correlation. The rapidity difference between p and $\bar{p}$ is shown in Fig. 8c. The rapidity y, defined as $y=1/2\ln((E+p_{\parallel})/(E-p_{\parallel}))$ where $p_{\parallel}$ is the momentum component parallel to the thrust axis, is less

than 1.06 for a maximum proton momentum of 1.2 GeV/c. Thus the maximal rapidity difference is limited to a value of about 2. The distribution in Fig. 8c has a maximum at a rapidity gap of zero and decreases almost linearly as Δy increases. Such a shape is consistent with the assumption of uncorrelated distributions of the proton and antiproton rapidities in the accessible range $-1.06 < y < 1.06$, although some degree of correlation cannot be excluded.

The data can be compared to the predictions of models by Meyer [16], the Lund group [17] and by Bell et al. [18] which is an extension of the model of Cerny et al. [19]. In the first two models, baryons are produced by the use of diquarks at a rate which is adjustable and which (in [17]) can be related to the masses of the diquarks. Reference [18] contains a longitudinal phase space model in which a randomisation of quark rapidities takes place [19] and in which baryons are produced by the local accumulation of quarks with similar rapidity.

The observed number of $p+\bar{p}$ events is consistent with the predictions of the models of [16, 17] which are tuned to reproduce the inclusive proton cross section in the momentum range 0.4–1.2 GeV/c (see [18]). The number of events with more than one $p+\bar{p}$ pair ($2p$, $2\bar{p}$, $2p+1\bar{p}$, $2\bar{p}+1p$ in Table 6) is consistent with a calculation assuming a Poisson distribution for nucleon-antinucleon pair production with an average value of $0.8 \pm 0.1\, p/\bar{p}$ per event (see above).

The predictions of the models of [16–18] are shown in Fig. 8a, b, c as solid, dashed and dashed-dotted lines respectively. The models by Meyer [16] and the Lund group [17] are consistent with all three distributions, whereas the phase space model of [18] predicts a peak at $\cos\theta_{p\bar{p}} = -1$ and a dip at $|y_p - y_{\bar{p}}| = 0$ in contradiction to the data. This dip arises from the quark recombination algorithm of [19] which prefers to produce mesons rather than a baryon-antibaryon pair overlapping in rapidity.

In summary, we measured cross sections for $\pi^{\pm}$, $K^{\pm}$ and $p, \bar{p}$ production over the full momentum range. We find that the fraction of $K^{\pm}$ and $p, \bar{p}$ increases with particle momentum, and that at a momentum of 5 GeV/c at $W = 34$ GeV (3 GeV/c at $W = 22$ GeV) the fractions $f_{\pi^{\pm}} : f_{K^{\pm}} : f_{p,\bar{p}}$ are roughly in the ratio 0.55:0.3:0.15. On average an event at $W = 34$ GeV contains $10.3 \pm 0.4\,\pi^{\pm}$, $2.0 \pm 0.2\,K^{\pm}$ and $0.8 \pm 0.1\, p, \bar{p}$. The available data on events containing more than one observed p or $\bar{p}$ show no statistically significant correlation between p and $\bar{p}$ within our restricted rapidity range of $|y| \leqq 1$. They are consistent with a class of models that assume for the fragmentation process both quarks and diquarks.

Acknowledgements. We wish to thank all persons at DESY and at the University of Hamburg, who contributed to the design, construction, and testing of the Cerenkov counters. We are particularly indebted to U. Balszuweit for producing the aerogel, to G. Krohn for assembling the Cerenkov counters, and to C.H. Sellmer for aluminizing the mirrors. We gratefully acknowledge the tremendous efforts of the PETRA machine group for the sustained high luminosity running. Those of us from abroad wish to thank the DESY directorate for the hospitality extended to us while working at DESY.

References

1. TASSO Collaboration R. Brandelik et al.: Phys. Lett. **113B**, 98 (1982)
2. TASSO Collaboration R. Brandelik et al.: Phys. Lett. **94B**, 444 (1980)
3. TASSO Collaboration R. Brandelik et al.: Phys. Lett. **105B**, 75 (1981); Phys. Lett. **94B**, 91 (1980)
4. PLUTO Collaboration Ch. Berger et al.: Phys. Lett. **104B**, 79 (1981)
5. JADE Collaboration W. Bartel et al.: Phys. Lett. **104B**, 325 (1981)
6. TASSO Collaboration R. Brandelik et al.: Phys. Lett. **113B**, 499 (1982)
7. TASSO Collaboration R. Brandelik et al.: Phys. Lett. **83B**, 261 (1979); H. Boerner et al.: Nucl. Instr. Meth. **176**, 151 (1980)
8. K.W. Bell et al.: Nucl. Instr. Meth. **179**, 27 (1981)
9. H. Burkhardt et al.: Nucl. Instr. Meth. **184**, 319 (1981); G. Poelz, R. Riethmüller: Nucl. Instr. Meth. **195**, 491 (1982)
10. TASSO Collaboration R. Brandelik et al.: Phys. Lett. **114B**, 65 (1982)
11. DASP Collaboration R. Brandelik et al.: Nucl. Phys. **B148**, 189 (1979); comparisons between measurements of identified particle cross sections in the c.m. energy range $5 \lesssim W \lesssim 10$ GeV are made in this reference as well as in D.G. Aschman et al.: Phys. Rev. Lett. **41**, 445 (1978), and H. Albrecht et al.: Phys. Lett. **102B**, 291 (1981)
12. M. Piccolo et al.: Phys. Lett. **86B**, 220 (1979); CLEO Collaboration A. Brody et al.: Phys. Rev. Lett. **48**, 1070 (1982)
13. G.S. Abrams et al.: Phys. Rev. Lett. **44**, 10 (1980); the values of $\langle n_{p,\bar{p}} \rangle$ were computed from their data on $R_{p,\bar{p}}$ using the total hadronic cross section given in M.W. Coles et al.: SLAC Report SLAC-PUB-2916 (1982), submitted for publication to Phys. Rev. D
14. M. Piccolo et al.: Phys. Rev. Lett. **39**, 1503 (1977)
15. P. Hoyer et al.: Nucl. Phys. **B161**, 349 (1979)
16. T. Meyer: Z. Phys. C – Particles and Fields **12**, 77 (1982)
17. B. Andersson et al.: Phys. Lett. **94B**, 211 (1980); Nucl. Phys. **B197**, 45 (1982)
18. K.W. Bell et al.: Rutherford Report RL-82-011 (1982)
19. V. Cerny, P. Lichard, J. Pisut: Phys. Rev. **D16**, 2822 (1977); Acta Phys. Polonica **B10**, 629 (1979); Phys. Rev. **D18**, 2409 (1978); Czech. J. Phys. **B31**, 1302 (1981)